





Article

Synthesis, Crystal Structures, Genotoxicity, and Antifungal and Antibacterial Studies of Ni(II) and Cd(II) Pyrazole Amide Coordination Complexes

Amal El Mahdaoui ¹, Smaail Radi ^{1,*}, Youssef Draoui ¹, Mohamed El Massaoudi ¹, Sabir Ouahhoud ^{2,3}, Abdeslam Asehraou ², Nour Eddine Bentouhami ², Ennouamane Saalaoui ², Redouane Benabbes ², Koen Robeyns ⁴ and Yann Garcia ^{4,*}

¹ LCAE, Department of Chemistry, Faculty of Sciences, University Mohammed I, Oujda 60000, Morocco; amalelmahdaoui2@gmail.com (A.E.M.); youssefx7draoui@gmail.com (Y.D.); elmassaoudio@gmail.com (M.E.M.)

² Laboratory of Bioresource Biotechnology Ethnopharmacology and Health, Faculty of Sciences, University Mohammed I, Oujda 60000, Morocco; sabir.ouahhoud@gmail.com (S.O.); a.asehraou@ump.ac.ma (A.A.); noureddine.bentouhami@ump.ac.ma (N.E.B.); e.saalaoui@ump.ac.ma (E.S.); r.benabbes@ump.ac.ma (R.B.)

³ Faculty of Medicine and Pharmacy, University Sultan Moulay Slimane, Beni Mellal 23000, Morocco

⁴ Institute of Condensed Matter and Nanosciences, Molecular Chemistry, Materials and Catalysis (IMCN/MOST), Université Catholique de Louvain, Place Louis Pasteur 1, 1348 Louvain-la-Neuve, Belgium; koen.robeyns@uclouvain.be

* Correspondence: s.radi@ump.ac.ma (S.R.); yann.garcia@uclouvain.be (Y.G.)



Citation: El Mahdaoui, A.; Radi, S.; Draoui, Y.; El Massaoudi, M.; Ouahhoud, S.; Asehraou, A.; Bentouhami, N.E.; Saalaoui, E.; Benabbes, R.; Robeyns, K.; et al. Synthesis, Crystal Structures, Genotoxicity, and Antifungal and Antibacterial Studies of Ni(II) and Cd(II) Pyrazole Amide Coordination Complexes. *Molecules* **2024**, *29*, 1186. <https://doi.org/10.3390/molecules29051186>

Academic Editors: Teodorico C. Ramalho and Antonio Zucca

Received: 2 February 2024
Revised: 25 February 2024
Accepted: 5 March 2024
Published: 6 March 2024



Copyright: © 2024 by the authors. Licensee MDPI, Basel, Switzerland. This article is an open access article distributed under the terms and conditions of the Creative Commons Attribution (CC BY) license (<https://creativecommons.org/licenses/by/4.0/>).

Abstract: In this study, we synthesized two coordination complexes based on pyrazole-based ligands, namely 1,5-dimethyl-*N*-phenyl-1H-pyrazole-3-carboxamide (**L**₁) and 1,5-dimethyl-*N*-propyl-1H-pyrazole-3-carboxamide (**L**₂), with the aim to investigate bio-inorganic properties. Their crystal structures revealed a mononuclear complex [Ni(**L**₁)₂](ClO₄)₂ (**C**₁) and a dinuclear complex [Cd₂(**L**₂)₂]Cl₄ (**C**₂). Very competitive antifungal and anti-Fusarium activities were found compared to the reference standard cycloheximide. Additionally, **L**₁ and **L**₂ present very weak genotoxicity in contrast to the observed increase in genotoxicity for the coordination complexes **C**₁ and **C**₂.

Keywords: pyrazole; amide; coordination complexes; antibacterial and antifungal activity; genotoxicity

1. Introduction

The growing problem of antibiotic resistance poses a significant threat to global health and food security. Bacteria are becoming increasingly resistant to commonly used antibiotics, forcing the use of less effective alternatives for treating common infections. This has led to the emergence of multi-drug-resistant pathogens, which the World Health Organization has identified as a major global health concern. Therefore, there is an immediate need to discover new types of medicines that can effectively fight these resistant strains [1,2].

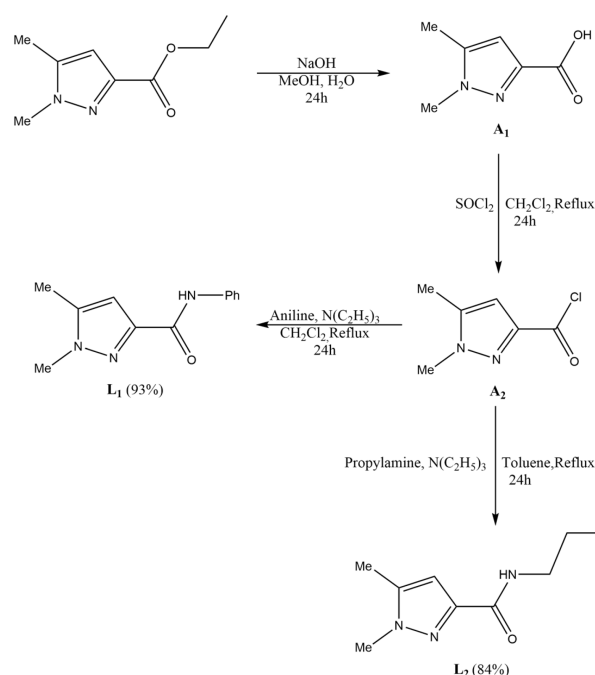
In the field of pharmaceuticals, most compounds, including lead structures, are typically organic in nature. This preference for organic compounds may seem obvious, given that metals and their compounds are primarily associated with industrial and catalytic applications and often linked to toxicity concerns. It is however interesting to note that metal-based coordination complexes have played vital roles in the history of medicine. Examples include arsenic's use in the first effective syphilis treatment (Salvarsan), mercury in the antiseptic mercurochrome and vaccine preservative thiomersal, or gold in treating rheumatoid arthritis (Auranofin) [3].

We recently turned our interest to pyrazole molecules due to their versatility and ability to engage in extensive interactions, making them particularly advantageous in the design and synthesis of metal–organic coordination compounds [4–13]. Such complexes could

be proposed for various applications such as metal ion extraction [14–16], catalysis [17], adsorbents of heavy metals [18–22], and corrosion inhibitors [23,24]. Additionally, pyrazole compounds have attracted considerable interest due to their broad spectrum of biological properties. These versatile compounds have shown significant potential as antibacterial, antifungal, anticancer, antioxidant, anti-inflammatory, antidepressant, antipyretic, antiviral, anti-tubercular, and anti-HIV agents [6,10–12,24–28]. The diverse range of biological effects exhibited by pyrazole molecules has made them a subject of extensive research in medicinal and pharmaceutical studies [29,30].

Metal complexes incorporating an amide functional group have gained considerable attention too. Amides possess broad biological properties and are utilized as effective chelating agents. Notably, amide groups incorporated into heterocyclic bases such as pyridine and pyrazine have emerged as a rapidly expanding class of ligand scaffolds that efficiently bind metal ions [31].

This study primarily focuses on the synthesis and characterization of two coordination complexes based on pyrazole amide ligands as antibiotic agents, namely 1,5-dimethyl-*N*-phenyl-1H-pyrazole-3-carboxamide (**L**₁, Scheme 1) and 1,5-dimethyl-*N*-propyl-1H-pyrazole-3-carboxamide (**L**₂). To do so, we examined the reactivity of **L**₁ in methanol with [Ni(H₂O)₆](ClO₄)₂ which led to a mononuclear complex [Ni(**L**₁)₂](ClO₄)₂ (**C**₁). Additionally, we explored the reactivity in methanol of **L**₂ with CdCl₂·2.5H₂O, which led to a dinuclear complex [Cd₂(**L**₂)₂]Cl₄ (**C**₂).



Scheme 1. Synthetic pathways leading to the formation of the ligands **L**₁ and **L**₂.

To assess the applicability of these compounds in real-world settings, their antibacterial and antifungal properties were studied. All compounds demonstrated antimicrobial activity against Gram (+) bacteria *Listeria innocua* and *Staphylococcus aureus*, as well as Gram (–) bacteria such as *Escherichia coli* and *Pseudomonas aeruginosa* and antifungal activity against pathogenic fungi *Geotrichum candidum*, *Aspergillus niger*, and *Penicillium crustosum*. Studying the genotoxicity of our compounds is also key to assessing their safety and evaluating their harmful effects for use cases in medicine, agriculture, and other applications. Minimal genotoxicity was observed for **L**₁ and **L**₂, but a significant rise in genotoxicity was exhibited for **C**₁ and **C**₂.

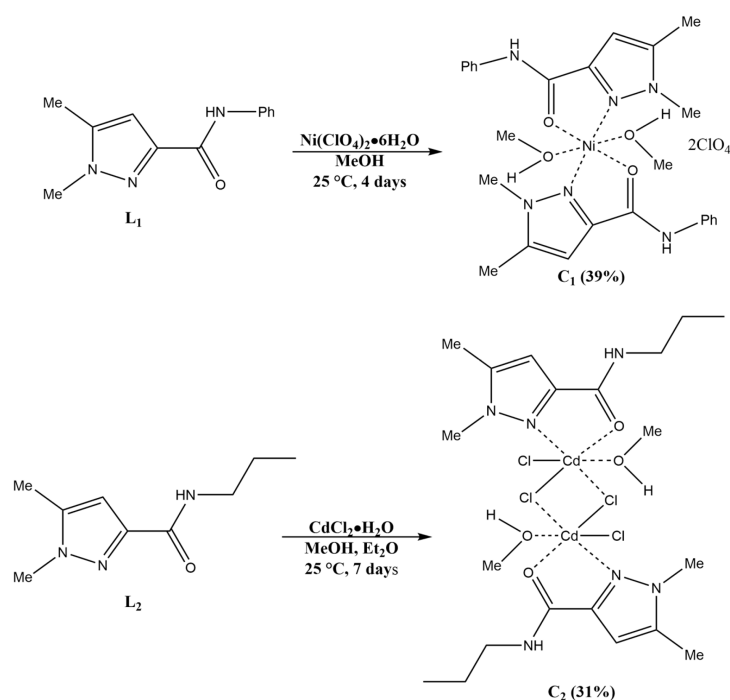
2. Results and Discussion

2.1. Synthesis of the Ligands

Since pyrazole has desirable biological properties, as outlined in the introduction, we used ethyl 1,5-dimethyl-1H-pyrazole-3-carboxylate as a starting point. Next, we performed the hydrolysis of the previous compound using methanol and NaOH to obtain 1,5-dimethyl-1H-pyrazole-3-carboxylic acid (**A**₁). In the following step, **A**₁ was dissolved in dichloromethane along with thionyl chloride SOCl₂ under stirring to obtain 1,5-dimethyl-1H-pyrazol-3-carbonyl chloride (**A**₂). The goal of the previous hydrolysis and chlorination steps was to be able to add the amide function to our compound, which is known to have desirable biological properties as mentioned in the introduction. In addition, **A**₂ (Scheme 1) was combined with a mixture of triethylamine and aniline in CH₂Cl₂. The mixture was heated at reflux for 24 h, filtered, and concentrated. The final product (**L**₁) was obtained as a white powder with a high yield (93%). Afterwards, **A**₂ was combined with a mixture of propylamine and triethylamine in toluene. The resulting mixture was refluxed for 24 h, filtered, and the solvent was removed. The crude product was purified via column chromatography on silica gel, affording **L**₂ as a white solid with a high yield (84%) (Scheme 1).

2.2. Synthesis of the Complexes

We aimed to investigate the influence of metal and counter anion selection on the formation and structural features of our coordination complexes, assessing their biological applications. To accomplish this, we utilized different ligand/metal ratios, experimented with diverse metal salts featuring varying counter anions, and employed various crystallization methods and solvents. From the compounds studied, **C**₁ and **C**₂ stood out as the most promising, producing high-quality single crystals suitable for X-ray analysis. The synthesis of the coordination complexes was conducted following Scheme 2. Here, a methanolic solution of Ni(ClO₄)₂·6H₂O was added to a methanolic solution of **L**₁. After four days of slow evaporation, blue single crystals of **C**₁ were obtained. A similar synthesis was carried out with **L**₂ and CdCl₂·H₂O. Vapor diffusion with diethyl ether led to colorless single crystals of **C**₂.



Scheme 2. Synthesis of the coordination complexes **C**₁ and **C**₂.

2.3. FT-IR Spectroscopy

Figure 1 reveals FT-IR spectra of L_1 , L_2 , and their respective coordination complexes C_1 and C_2 . The purpose of this analysis was to observe the distinctive bands of the ligands and track their shifts upon coordination with the transition metals. Characteristic bands ($2949(1) \text{ cm}^{-1}$) of the aromatic C-H are observed in both L_1 and L_2 . Additionally, bands at 3279 cm^{-1} and 3276 cm^{-1} for L_1 and L_2 , respectively, reveal N-H vibrations of the amine groups. Additionally, amide C=O bands are observed at 1658 cm^{-1} and 1685 cm^{-1} for L_1 and L_2 , respectively. Furthermore, $\sim 1537 \text{ cm}^{-1}$ corresponds to C=C aromatic stretching in both L_1 and L_2 . C-O vibrations of the alkyl group function in L_2 are detected at 1037 cm^{-1} and 1241 cm^{-1} .

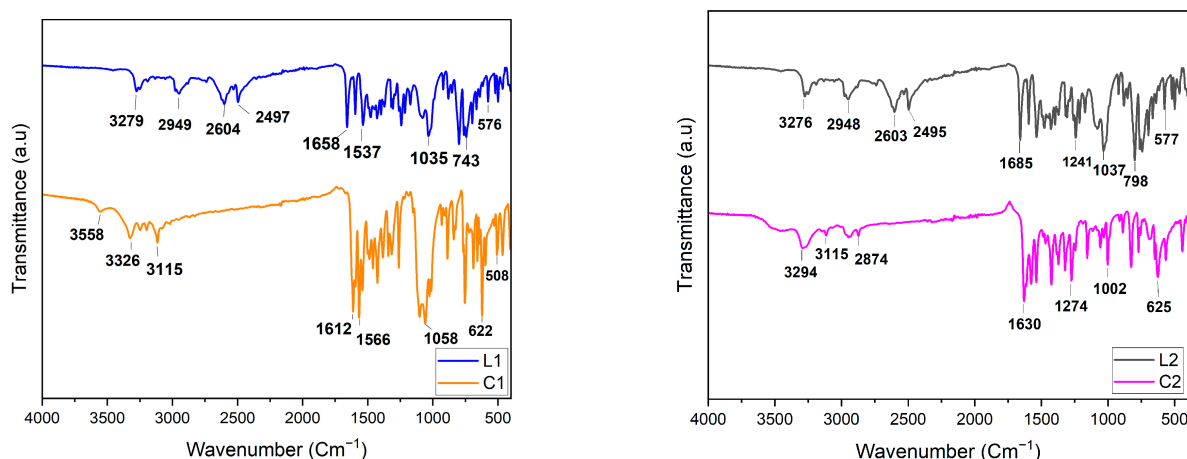


Figure 1. FTIR spectroscopy comparison plot of L_1 , C_1 (left panel) and L_2 , C_2 (right panel).

By comparing L_1 , C_1 and L_2 , C_2 , respectively, a shift in the bands is systematically observed, which points to metal coordination. Furthermore, the peak at 1058 cm^{-1} becomes stronger in C_1 compared to L_1 , which can be explained by the presence of non-coordinating perchlorate anions [32]. Using FT-IR, we were unable to observe bands corresponding to Cd-O, Cd-N, Ni-O, and Ni-N, which are theoretically expected below 500 cm^{-1} [33–35]. However, we were able to confirm the formation of the respective complexes by X-ray crystallography.

2.4. X-ray Crystallography

L_1 crystallizes in the orthorhombic system, in space group $Pbca$ (#61). The asymmetric unit contains one ligand L_1 ($Z = 8$). A single hydrogen bond between the N-H and C=O propagates along the b -axis (Figure 2a). Complex C_1 crystallizes in the monoclinic system, in space group $P2_1/n$ (#14). The crystal structure shows a nickel mononuclear complex, the metal ion being coordinated by two bidentate chelating L_1 ligands in the equatorial position and two methanol molecules in axial positions (Figure 2b). The complex is perfectly symmetrical, with the Ni atom found at a crystallographic inversion center; the asymmetric unit consists thus of half a C_1 nickel complex with a single perchlorate as a counter anion ($Z' = 0.5$).

Complex C_2 crystallizes in the orthorhombic system, in space group $Pca2_1$ (#29). The asymmetric unit consists of two dinuclear complexes, one being solvated with two methanol molecules, giving an octahedral geometry around the Cd atoms, the other without any coordinated solvent molecules, giving a square pyramidal geometry for the Cd atoms. In either case, the Cd centers are complexed with a bidentate chelating L_2 ligand, one chloride anion, and two bridging chloride anions with a 3.74 \AA Cd...Cd separation distance for the desolvated complex and a 3.60 \AA Cd...Cd separation dinuclear for the solvated dinuclear complex.

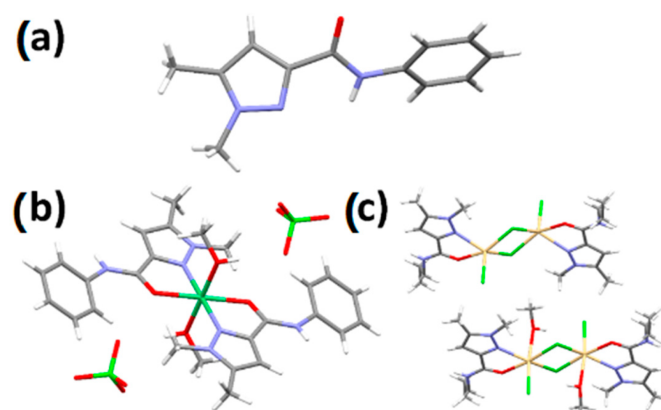


Figure 2. View of the molecular structures of L_1 (a), $[\text{Ni}(L_1)_2](\text{ClO}_4)_2$ (C_1), (b) and $[\text{Cd}_2(L_2)_2]\text{Cl}_4$ (C_2) (c). Disorder was omitted for clarity.

2.5. Antibacterial Activity

Screening of the antibacterial activities of L_1 , L_2 , C_1 , and C_2 against Gram (+) (*Listeria innocua* and *Staphylococcus aureus*) and Gram (−) (*Escherichia coli* and *Pseudomonas aeruginosa*) bacteria was undertaken. Interestingly, there is an increase in the inhibition of C_1 and C_2 compared to L_1 and L_2 , respectively, despite the lower concentration of the coordination complexes (see Figure 3 and Table 1). This enhanced performance can be attributed primarily to the influence of transition metals, which increase the lipophilicity of the coordination complexes compared to organic molecules [36]. As a result, the lipid membrane bilayer becomes more permeable to these complexes, facilitating their transfer [36]. This effect is more pronounced for C_2 compared to L_2 . C_2 provides the highest inhibition compared to L_1 , L_2 and C_1 on all bacteria tested. C_2 displays a 16.1 mm inhibition zone on *E. coli*, which is half of the inhibition zone provided by the control, Gentamicin. It is therefore higher than the dinuclear complex $[\text{Cd}_2(\text{dmamp})_2(\text{NCS})_2]_n$ (where $\text{dmamp} = 2-[(2\text{-dimethylaminoethylimino)methyl}]phenol$) [37] and of the same range as another dinuclear complex, CdL_2Cl_2 , where $L = 2-(3,5,5'\text{-trimethyl-1'H-[1,3'-bipyrazol]-1'-yl})acetoneitrile$ [38] (see Table 1). This result could be attributed to the superior antibacterial activity of pyrazole. Finally, note that Cd and Ni salts used in the synthesis of our coordination complexes display a weak antibacterial activity [38] that does not significantly affect the activity of our coordination complexes (see Table 1).

Table 1. Inhibition zones (mm) of bacterial targets obtained with L_1 , L_2 , C_1 , C_2 , and other reference compounds.

| Compound | C (mmol/L) | Inhibition Zone (mm) | | | | Ref. |
|--|------------|----------------------|------------------------|---------------------------|----------------------|-----------|
| | | <i>E. coli</i> [n] | <i>Li. Innocua</i> [p] | <i>Ps. Aeruginosa</i> [n] | <i>S. Aureus</i> [p] | |
| L_1 | 27.8 | $9.20 \pm 0.53^*$ | $7.94 \pm 0.40^*$ | $9.17 \pm 1.04^*$ | $8.17 \pm 0.76^*$ | This work |
| C_1 | 7.98 | $9.65 \pm 0.28^*$ | $10.20 \pm 0.28^*$ | $10.15 \pm 0.28^*$ | $10.6 \pm 0.28^*$ | This work |
| L_2 | 33.1 | $9.30 \pm 0.17^*$ | $8.33 \pm 1.15^*$ | $9.17 \pm 0.85^*$ | $7.10 \pm 1.56^*$ | This work |
| C_2 | 7.88 | $16.10 \pm 0.28^*$ | $14 \pm 0.28^*$ | $14.7 \pm 0.57^*$ | $12.8 \pm 0.28^*$ | This work |
| Gentamicin | 1.25 | 29.9 ± 0.28 | 30.10 ± 0.28 | 27.75 ± 0.35 | 32.85 ± 0.70 | This work |
| $[\text{Cd}_2(\text{dmamp})_2(\text{NCS})_2]_n$ | --- | 9.2 | -- | 13.1 | -- | [37] |
| $[\text{Ni}(\text{btbepa})\text{CH}_3\text{OH}(\text{H}_2\text{O})](\text{ClO}_4)_2$ | -- | 28 | -- | -- | 27 | [6] |
| $\text{H}_3\text{O}[\text{Ni}(\text{dmptr})_3](\text{ClO}_4)_3$ | 4.62 | 12 ± 0.38 | -- | -- | 12 ± 0.25 | [32] |
| $[\text{Cd}(\text{dmptr})_2\text{Cl}_2]$ | 7.85 | 27 ± 0.25 | -- | -- | 27 ± 0.19 | [32] |

Table 1. Cont.

| Compound | C (mmol/L) | Inhibition Zone (mm) | | | | Ref. |
|---|------------|-------------------------------|-----------------------------------|--------------------------------------|---------------------------------|------|
| | | <i>E. coli</i> ^[n] | <i>Li. Innocua</i> ^[p] | <i>Ps. Aeruginosa</i> ^[n] | <i>S. Aureus</i> ^[p] | |
| [Cd(htcd)(SCN)]SCN | -- | 22 | -- | -- | 24 | [39] |
| [NiL ₃](ClO ₄) ₂ | 3.49 | 8 ± 0.8 | 9 ± 0.35 | 9 ± 0.95 | 8 ± 0.35 | [38] |
| CdL ₂ Cl ₂ | 5.25 | 14 ± 0.75 | 11 ± 0.5 | 12 ± 0.3 | 11 ± 0.5 | [38] |
| Ni(ClO ₄) ₂ ·6H ₂ O | 8.2 | 0 | 0 | 0 | 0 | [38] |
| CdCl ₂ ·H ₂ O | 14.9 | 11 ± 0.3 | 0 | 8 ± 0.2 | 0 | [38] |

[p]: Gram positive; [n]: Gram negative. * $p < 0.05$ compared with Gentamicin. dmamp = 2-[(2-dimethylaminoethylimino)methyl]phenol). btbepa = *N,N*-bis(2-(10,5,50-trimethyl-1H,10H-[3,30-bipyrazol]-1-yl)ethyl)propan-1-amine. dmpr = 3-(3,5-dimethyl-1H-pyrazol-1-yl)-1H-1,2,4-triazole. htcd = 5,7,7,12,14,14-hexamethyl-1,4,8,11-tetraazacyclotetradeca-4,11-diene. L = 2-(3,5,5'-trimethyl-1'H-[1,3'-bipyrazol]-1'-yl)acetonitrile.

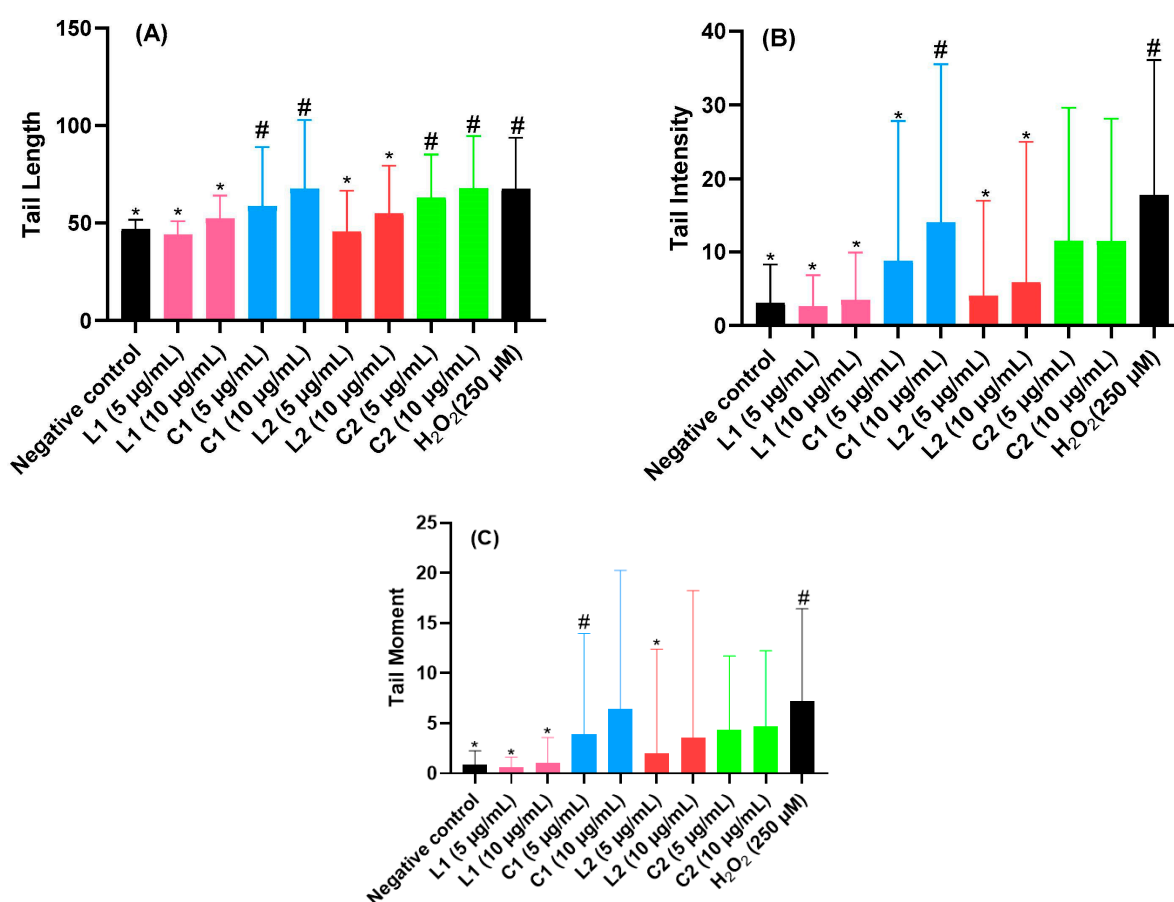


Figure 3. Assessment of the impact of L₁, L₂ and C₁, C₂ on (A) DNA tail length, (B) the percentage of tail intensity, and (C) DNA tail moment in rat leukocytes. Results presented as means ± SEM (50 cells × 2). # $p < 0.05$ compared with negative control; * $p < 0.05$ compared with H₂O₂.

2.6. Antifungal Activity

We now focus our attention on the antifungal activity of our ligands and complexes against *Geotrichum candidum*, *Aspergillus niger*, and *Penicillium crustosum*. Coordination complexes C₁ and C₂ exhibit a noticeable increase in the inhibition zone compared to both L₁ and L₂ (Table 2), similar to the observed behavior in the previous section for the antibacterial activity. Additionally, the antifungal activity of C₁ and C₂ is generally comparable to that of cycloheximide. In particular, the inhibition zone of C₂ against *A. niger* (24.5 ± 0.71 mm) and *P. crustosum* (26 ± 2.83 mm) is slightly higher, with statistical significance ($p < 0.05$), compared to the reference cycloheximide [40]. This result confirms that C₂ has a very strong

antifungal attitude. Additionally, **C**₂ also has comparable antifungal activity compared to a Ni coordination complex [41] and a superior activity compared to other Cd and Ni coordination complexes [38,42–44] (see Table 2). Similar to the antibacterial activities, note that Cd and Ni salts only show a weak antifungal activity [38] (see Table 2).

Table 2. Inhibition zones (mm) of fungal targets obtained with **L**₁, **L**₂, **C**₁, and **C**₂ and comparison with the literature.

| Compound | C (mmol/L) | Inhibition Zone (mm) | | | Ref. |
|---|---------------|----------------------|-----------------|---------------------|-----------|
| | | <i>G.candidum</i> | <i>A. niger</i> | <i>P. crustosum</i> | |
| L ₁ | 27.87 | 13.9 ± 0.1 * | 10.25 ± 0.75 * | 8.8 ± 0.2 * | This work |
| C ₁ | 7.98 | 15.5 ± 0.71 * | 19 ± 1.41 * | 22 ± 1.41 | This work |
| L ₂ | 33.11 | 12.5 ± 0.6 * | 9.85 ± 0.65 * | 8.25 ± 0.25 * | This work |
| C ₂ | 7.88 | 20 ± 1.41 * | 24.5 ± 0.71 * | 26 ± 2.83 * | This work |
| Cycloheximide | 21.33 | 22.8 ± 0.2 | 22.7 ± 0.5 | 22.6 ± 0.6 | This work |
| Cycloheximide (lower concentration) | 10.66 | 22 ± 0.8 | 22 ± 0.7 | 22 ± 0.6 | This work |
| [Ni(IND) ₂ (Gly)(H ₂ O) ₂]Cl | -- | 22.7 ± 0.03 | -- | -- | [41] |
| Cd(bdade)(NCS) ₂ | -- | -- | 18.44 | -- | [42] |
| [Ni(ψ) ₂ SO ₄] | -- | -- | 10 | -- | [43] |
| [Ni(CH ₃ COO) ₂ (Tyr) ₂] Tyr = Tyrosine | -- | -- | 23 | -- | [45] |
| [NiL ₃](ClO ₄) ₂ | 3.49 | 0 | 9 | 9 ± 0.1 | [38] |
| CdL ₂ Cl ₂ | 5.25 | 14 ± 0.2 | 14 ± 0.8 | 15 ± 0.45 | [38] |
| Ni(ClO ₄) ₂ ·6H ₂ O | 8.2 | 0 | 0 | 0 | [38] |
| CdCl ₂ ·H ₂ O | 14.9 | 10 ± 0.1 | 6 ± 0.3 | 5 ± 0.2 | [38] |

* $p < 0.05$ compared with cycloheximide (T+). IND = indapamide; Gly = glycine; bdade = bis(3(4-dimethylaminophenyl)-allylidene)-1,2-diaminoethane; ψ = hydrazine carboxamide, 2-[3-methyl-2-thienylmethylene]; L = 2-(3,5,5'-trimethyl-1'H-[1,3'-bipyrazol]-1'-yl) acetonitrile.

2.7. Antifungal Activity on Mycelial Growth of *Fusarium oxysporum* f. sp. *Albidis*

Our ligands and coordination complexes display anti-*Fusarium* properties in contrast to cycloheximide (see Table 3), but our coordination complexes show stronger anti-*Fusarium* properties compared to the ligands even though our complexes were used in lower concentrations. In particular, **C**₂ exhibits a remarkable inhibition of 96% even at low concentrations (78.9 μmol/L) compared to all other compounds, including cycloheximide. Its characteristics overcome reported values for ligand molecules [46,47] in addition to other Cd and Ni coordination complexes (Table 3). The anti-*Fusarium* inhibition activity of our **C**₂ is also comparable to the remarkable inhibition properties of two dinuclear Co and Cu complexes reported recently [38,44]. Remarkably, the Cd and Ni salts used for the synthesis of our coordination complexes have a weak anti-*Fusarium* activity [38] (Table 3).

2.8. Genotoxicity

To assess the genotoxicity of **L**₁ and **L**₂ as well as of the coordination complexes **C**₁ and **C**₂, we report the tail intensity, tail length, and tail moment (see Figure 3). For the sake of comparison, we compare their genotoxicity with hydrogen peroxide, which is known for being a typical DNA-damage-inducing agent [47]. **L**₁ and **L**₂ have weak genotoxicity compared to the negative control, whereas an increase in genotoxicity is found for **C**₁ and **C**₂ in comparison to hydrogen peroxide. This effect is likely due to the fact that Ni and Cd have a relatively high genotoxic activity [48,49]. Note that Cd is a toxic metal that accumulates in tissues and can cause genotoxic effects, including DNA damage and chromosomal aberrations, and disrupt DNA repair mechanisms. Additionally, Cd inhibits DNA methylation, altering gene expression patterns. Chronic exposure to cadmium is associated with an increased cancer risk [50]. Nickel, widely used in industries like stainless steel production, is classified as a human carcinogen. It induces genotoxic effects through

DNA damage, chromosomal aberrations, and interference with DNA repair mechanisms, particularly in occupations such as mining and welding [51].

Table 3. Antifusarium activities of L₁, L₂, C₁, C₂, and reference compounds for different sample volumes.

| Compound | Sample Volumes (μL) | C (μmol/L) | Inhibition (%) | Ref. |
|--|---------------------|------------|----------------|-----------|
| L ₁ | 50 | 92.9 | 46.3 ± 2.5 * | This work |
| | 150 | 278.7 | 50 ± 4.5 | |
| C ₁ | 50 | 26.6 | 43.8 ± 3.3 | This work |
| | 150 | 79.8 | 62.5 ± 2.2 * | |
| L ₂ | 50 | 110.35 | 50 ± 7.8 * | This work |
| | 150 | 331.05 | 57.5 ± 6.6 | |
| C ₂ | 50 | 26.3 | 87.5 ± 3.3 * | This work |
| | 150 | 78.9 | 96.3 ± 1.3 * | |
| Cycloheximide | 50 | 71.1 | 35 ± 3.3 | This work |
| | 150 | 213.3 | 55 ± 2.5 | |
| | 250 | 355.5 | 66.7 ± 2.9 | |
| Cd(dmptr) ₂ Cl ₂ | 200 | 104.6 | 50 | [32] |
| (H ₃ O)[Ni(dmptr) ₃](ClO ₄) ₃ | 200 | 29.41 | 38 | [32] |
| [Ni(btbeпа)CH ₃ OH(H ₂ O)](ClO ₄) ₂ | 200 | 68.8 | 44 | [6] |
| NiL ₃ (ClO ₄) ₂ | 150 | 66.42 | 35 | [38] |
| CdL ₂ Cl ₂ | 150 | 97.75 | 51 | [38] |
| Co ₂ (HL ₂)L ₂ Cl ₃ | 150 | 81.1 | 97 | [38] |
| Cu ₂ (HL ₂)Cl ₂ | 150 | 158.02 | 97 | [44] |
| Ni(ClO ₄) ₂ ·6H ₂ O | 150 | 164.07 | 8 | [38] |
| CdCl ₂ ·H ₂ O | 150 | 298.01 | 12 | [38] |

* $p < 0.05$ compared to cycloheximide (T+), btbeпа = *N,N*-bis(2-(10,5,50-trimethyl-1H,10 H-[3,30-bipyrazol]-1-yl)ethyl) propan-1-amine; dmptr = 3-(3,5-dimethyl-1H-pyrazol-1-yl)-1H-1,2,4-triazole; L = 2-(3,5,5'-trimethyl-1'H-[1,3'-bipyrazol]-1'-yl)acetonitrile; HL₂ = 1'-((1H-tetrazole-5-yl)methyl)-3,5,5'-trimethyl-1'H-1,3'-bipyrazole; HL₂' = 5-((3-(3,5-dimethyl-1H-pyrazol-1-yl)-1H-1,2,4-triazol-1-yl)methyl)-406 1H-tetrazole.

3. Experimental Section

3.1. Materials and Instrumentation

Commercially available analytical-grade solvents and chemicals were used without any additional purification steps. ¹H and ¹³C NMR spectra were acquired using a Bruker AC 300 spectrometer (Bruker, Billerica, MA, USA). ESI ionization was employed to acquire HRMS data using a Q Exactive ion trap spectrometer from Thermo Fisher Scientific (Waltham, MA, USA), enabling high-resolution mass spectrometry measurements for C₁ and C₂. For the compounds L₁ and L₂, we used a low-resolution (LXQ) ESI MS. FT-IR spectra were recorded on a JASCO FT/IR-4700 spectrometer (JASCO, Lexington, KY, USA) using an ATR attachment. Melting points were measured using a Koffler bench. Elemental analyses were performed using a EuroEA Elemental Analyzer (HEKAtech GmbH, Wegberg, Germany).

3.2. Synthesis Section

3.2.1. Synthesis of Ethyl 1,5-Dimethyl-1H-pyrazole-3-carboxylate

Ethyl 5-methyl-1H-pyrazole-3-carboxylate 10 g (65 mmol) and tBuOK 7.9g (65 mmol) were introduced into anhydrous diethyl ether (230 mL). The reaction mixture was then heated under reflux for 1 h, and subsequently cooled using ice. Next, a solution of methyl iodide was added dropwise, and the mixture was refluxed for 4 h, then filtered and concentrated to dryness. To the resulting oil, 25 mL of hexane was added, and the solution

was placed in a refrigerator overnight. The product obtained after filtration was in the form of yellowish crystals. M.p: 45 °C. Yield: 77 % (7.5 g). ¹H-NMR (CDCl₃) δ ppm: 1.40 (t, 3H, CH₂-CH₃), 2.33 (s, 3H, -CH₃), 3.90 (s, 3H, N-CH₃), 4.35 (q, 2H, CH₂-CH₃), (s, 1H, Pz-H). IR (KBr, v(cm⁻¹)): 1690 (C=O).

3.2.2. Synthesis of 1,5-Dimethyl-1H-pyrazole-3-carboxylic Acid (A₁)

Ethyl 1,5-dimethyl-1H-pyrazole-3-carboxylate (2 g, 11.89 mmol) and methanol (20 mL) were added to a NaOH (0.95 g, 23 mmol) aqueous solution (30 mL). The resulting mixture was stirred for 24 h. After cooling to 0 °C, it was neutralized using dilute HCl, leading to a white precipitate. The precipitate was separated by filtration, washed with water (15 mL), and dried in a desiccator. M.p: 190 °C. Yield: 90% (1.8 g). ¹H-NMR (DMSO-d₆) δ ppm: 2.23 (s, 3H, C-C), 3.75 (s, 3H, C-N), 6.44 (s, 1H, C=CH-C). ¹³C-NMR (DMSO-d₆) δ ppm: 11.2 (C-C-N), 37.1 (C-N-N), 108.3 (C=CH-C), 140.7 (C=C=C), 142.1 (CH-C=O), 163.9 (C-C-OH).

3.2.3. Synthesis of 1,5-Dimethyl-1H-pyrazol-3-carbonyl Chloride (A₂)

A₁ (2 g, 14.27 mmol) was dissolved in dichloromethane, CH₂Cl₂ (40 mL). Under stirring, thionyl chloride SOCl₂ (2 mL) was added, and the mixture was heated to 90 °C for 24 h. Afterwards, the mixture was cooled. When CH₂Cl₂ and SOCl₂ had completely evaporated, the resulting white solid was dissolved in dichloromethane and distilled water. The solution was then neutralized with sodium bicarbonate until reaching a pH = 5. The mixture was decanted using a separating funnel, and the organic phase was subsequently extracted with dichloromethane (20 mL). It was then dried using sodium sulfate and evaporated to dryness. A white solid was obtained. M.p: 80 °C. Yield: 70% (1.7 g). ¹H-NMR (CDCl₃) δ ppm: 2.16 (s, 3H, C-C), 3.84 (s, 3H, C-N), 6.59 (s, 1H, C=CH-C). ¹³C-NMR (CDCl₃) δ ppm: 11.3 (C-C-N), 37.5 (C-N-N), 110.0 (C=CH-C), 141.5 (C=C=C), 142 (CH-C=O), 162 (C-C-Cl).

3.2.4. Synthesis of 1,5-Dimethyl-N-phenyl-1H-pyrazole-3-carboxamide (L₁)

A solution of A₂ (1 g, 6.30 mmol) (20 mL) was mixed with triethylamine (0.87 mL) and aniline (0.56 mL) in dichloromethane (10 mL), which was added slowly. The resulting mixture was heated at reflux for 24 h, followed by filtration, and was then cooled to room temperature and concentrated to dryness. The expected product was precipitated in petroleum ether and was purified by recrystallization in petroleum ether, resulting in a white powder. M.p: 150 °C. Yield: 93% (0.97 g). FT-IR: 3279(w), 2949(w), 2604(w), 2497(w), 1658 (s), 1537(s), 1035(s), 743(m), 576(w). ¹H-NMR (CDCl₃) δ ppm: 2.23 (s,3H, C-C), 3.74 (s, 3H, C-N), 6.55 (s, 1H, C=CH-C), 7.03 (t, 1H, CH=CH-CH), 7.27 (t, 1H, CH=CH-CH), 7.61 (d, 1H, C-CH=CH), 8.61 (s, 1H, NH-C). ¹³C-NMR (CDCl₃) δ ppm: 11.3 (C-C-N), 36.6 (C-N-N), 106.4 (C=CH-C), 119.5 (C-CH=CH), 123.8 (CH-CH=CH), 128.9 (CH=CH-CH), 138.1 (NH-C-CH), 140.7 (C-C=CH), 145.1 (N=C-CH), 159.9 (O=C-NH). MS (ESI) (Methanol): *m/z* = 216 [M+H]⁺ (calc. 215.2), (see Figures S1, S2 and S5).

3.2.5. Synthesis of 1,5-Dimethyl-N-propyl-1H-pyrazole-3-carboxamide (L₂)

To a solution of A₂ (0.60 g, 3.78 mmol) in dry toluene (10 mL) at 0 °C, a mixture of propylamine (0.65 mL, 3.73 mmol) and triethylamine (0.52 mL, 3.75 mmol) in toluene (20 mL) was slowly added. The resulting mixture was heated at reflux for 24 h. The reaction mixture was then filtered, and the solvent was removed under reduced pressure. The crude product was purified via column chromatography on silica gel (EtOAc/Hexane: 5/5), resulting in a white solid. M.p 72 °C. Yield 84% (0.51 g). FT-IR: 3276(w), 2948(w), 2603(w), 2495(w), 1685(s), 1241(m), 1037(s), 798(s), 577(w). ¹H-NMR (DMSO) δ ppm: 0.83 (t, 3H, C-C), 1.47 (m, 2H, C-C-C), 2.25 (s, 3H, C-C), 3.14 (m, 2H, NH-C-C), 3.75 (s, 3H, C-N), 6.37 (s, 1H, C=CH-C), 7.92 (t, 1H, C-NH-C). ¹³C-NMR (DMSO) δ ppm: 11.3 (C-C-N), 11.9 (C-C), 23.1 (C-C-C), 36.8 (C-N-N), 40.6 (NH-C-C), 105.8 (C=CH-C), 140.6 (C-C=CH), 145.5 (N=C-C=O), 162.0 (O=C-NH). MS (ESI) (Methanol): *m/z* = 182 [M+H]⁺ (calc.181.2), (see Figures S3, S4 and S6).

3.2.6. Synthesis of $[\text{Ni}(\text{L}_1)_2](\text{ClO}_4)_2$ (C_1)

L_1 (43.1 mg, 0.2 mmol, 2 equiv.) was dissolved in methanol (3 mL). $\text{Ni}(\text{ClO}_4)_2 \cdot 6\text{H}_2\text{O}$ (36.6 mg, 0.1 mmol, 1 equiv.) was dissolved in methanol (3 mL) and added to the previous solution of L_1 . The mixture was stirred for 10 min at room temperature. After 4 days of slow evaporation, blue single crystals were obtained. Yield: 39% (29 mg). FT-IR: 3558(w), 3326(w), 3115(w), 1612 (s), 1566(s), 1058(s), 622(s), 508(m). HRMS (ESI) (CH_3OH): $m/z = 244.07280$ [$\text{C}_{24}\text{H}_{26}\text{O}_2\text{N}_6^{58}\text{Ni}$], (see Figure S7).

3.2.7. Synthesis of $[\text{Cd}_2(\text{L}_2)_2]\text{Cl}_4$ (C_2)

L_2 (36.2 mg, 0.1 mmol, 3 equiv.) was dissolved in methanol (3 mL). $\text{CdCl}_2 \cdot \text{H}_2\text{O}$ (24.2 mg, 0.1 mmol, 1 equiv.) was dissolved in methanol (3 mL), with the addition of five drops of water, and then added to the previous solution of L_2 . The mixture was stirred for 10 min at room temperature. The resulting clear liquid mixture was subjected to vapor diffusion with diethyl ether (10 mL) at room temperature. After 7 days, colorless crystals were obtained. Yield: 31% (21 mg). FT-IR: 3294(w), 3115(w), 2874(w), 1630(s), 1274(s), 1002(m), 625(s). HRMS (ESI) (CH_3OH): $m/z = 234.07423$ [$\text{C}_{18}\text{H}_{30}\text{O}_2\text{N}_6^{106}\text{Cd}$], (see Figure S8).

3.3. X-ray Crystallographic Studies

Diffraction data for L_1 , C_1 , and C_2 were collected on an MAR345 Image plate detector using a monochromated (Montel optics) microfocus Mo- $\text{K}\alpha$ radiation ($\lambda = 0.71073 \text{ \AA}$) source (Incoatec I μ S). Data integration and reduction were performed using the CrysAlis^{PRO} V 1.171.37.35 crystallographic software package and absorption correction was used [52].

The structures were solved by dual-space direct methods (SHELXT) [53] and refined by full matrix least squares on F^2 using SHELXL [54]. All non-hydrogen atoms were refined anisotropically and hydrogen atoms were placed at the calculated positions with isotropic temperature factors fixed at 1.2 times the U_{eq} of the parent atoms (1.5 U_{eq} for methyl and OH hydrogens).

In L_1 , methyl hydrogens showed rotational disorder and were refined as an idealized disordered methyl group with two positions rotated by 60° . In C_1 , the Ni complex showed whole-molecule disorder. The octahedral Ni complex consists of two L_1 ligands in the equatorial plane with two methanol molecules in the axial positions, giving a perfectly symmetrical complex, with the Ni atom found at an inversion center. The disorder consists of a 90° rotation of the ligands within the same equatorial plane with a refined ratio of about 84/16. Additionally, the perchlorate anion is also disordered over two discrete positions in a 90/10 ratio. In C_2 , both dinuclear complexes in the asymmetric unit show disorder of the Cd cations, and, as a result, so do the coordinated Cl anion and methanol. The asymmetric unit could be seen as a mixture of the solvated dinuclear complex and the desolvated structure. As the overall geometrical differences between both structures are relatively small, both can be interchanged. As no deterioration of the diffraction was observed, it is less likely that the observed structure is an averaged structure where solvent evaporation occurred at the surface of the crystal during the measurement at ambient conditions, as this would result in non-stoichiometric ratios of both dinuclear complexes. Also, one of the propyl chains in both dinuclear complexes showed disorder that could be refined in two discrete positions in a 90/10 ratio.

Details of the crystallographic and refinement details for the compounds are listed in Table 4. CCDC 2290595-2290597 contain the supplementary crystallographic data for this paper. These data can be obtained free of charge from The Cambridge Crystallographic Data Centre via www.ccdc.cam.ac.uk/structures.

Table 4. Crystal data and structure refinement for L₁, C₁, and C₂.

| Compound | L ₁ | C ₁ | C ₂ |
|--|---|---|--|
| Empirical formula | C ₁₂ H ₁₃ N ₃ O | C ₂₆ H ₃₄ Cl ₂ N ₆ Ni O ₁₂ | C ₃₈ H ₆₈ Cd ₄ Cl ₈ N ₁₂ O ₆ |
| Formula weight | 215.25 | 752.20 | 1522.24 |
| T (K) | 293(2) | 293(2) | 293(2) |
| Wavelength (Å) | 0.71073 | 0.71073 | 0.71073 |
| Crystal system | Orthorhombic | Monoclinic | Orthorhombic |
| Space group | <i>Pbca</i> | <i>P2₁/n</i> | <i>Pca2₁</i> |
| Unit cell dimensions (Å, °) | a = 10.4982(4) b = 9.8653(4) c = 21.4838(9) α = 90 β = 90 γ = 90 | a = 10.6244(6) b = 13.0110(7) c = 11.8231(7) α = 90 β = 96.503(6) γ = 90 | a = 16.7846(3) b = 16.4470(3) c = 20.9709(3) α = 90 β = 90 γ = 90 |
| V (Å ³) | 2225.04(15) | 1623.84(16) | 5789.16(16) |
| Z | 8 | 2 | 4 |
| Density (calculated) (g/cm ³) | 1.285 | 1.538 | 1.747 |
| Absorption coefficient (mm ⁻¹) | 0.085 | 0.832 | 1.869 |
| F(000) | 912 | 780 | 3024 |
| Crystal size (mm ³) | 0.32 × 0.15 × 0.12 | 0.35 × 0.30 × 0.20 | 0.40 × 0.25 × 0.20 |
| θ range for data collection (°) | 2.988 to 26.193 | 2.902 to 26.232 | 2.893 to 26.187 |
| Reflections collected | 16410 | 11040 | 39165 |
| Independent reflections | 2215 [R(int) = 0.0480] | 3199 [R(int) = 0.0253] | 11,407 [R(int) = 0.0185] |
| Completeness to θ 25.242° (%) | 99.2 | 98.9 | 98.9 |
| Max. and min. transmission | 1.00000 and 0.82569 | 1.00000 and 0.88273 | 1.00000 and 0.66350 |
| Data/restraints/parameters | 2215/0/147 | 3199/99/273 | 11407/43/721 |
| Goodness-of-fit on F ² | 1.086 | 1.045 | 1.070 |
| Final R indices [I > 2s(I)] | R1 = 0.0441, wR2 = 0.1216 | R1 = 0.0374, wR2 = 0.1059 | R1 = 0.0188, wR2 = 0.0486 |
| R indices (all data) | R1 = 0.0488, wR2 = 0.1254 | R1 = 0.0398, wR2 = 0.1079 | R1 = 0.0197, wR2 = 0.0490 |
| Absolute structure parameter | . | . | 0.31(2) |
| Δρ(max, min)(e.Å ⁻³) | 0.187, −0.170 | 0.411, −0.289 | 0.528, −0.371 |

4. Biological Activity

4.1. Microorganisms and Culture Media

The bacterial strains utilized in this work were two Gram-positive (*Staphylococcus aureus* (*S. aureus*) and *Listeria innocua* (*Li. innocua*)) and two Gram-negative bacteria (*Pseudomonas aeruginosa* (*Ps. aeruginosa*) and *Escherichia coli* (*E. coli*)). These bacterial strains are involved in foodborne illnesses. The fungal strains tested in this work were *Asperillus niger*, *Geotrichum candidum*, and *Penicillium crustosum*. These fungi are involved in postharvest diseases of fruits and vegetables, and they can be associated with the production of mycotoxins, which are dangerous for human and animal health. All these microorganisms are available in the Laboratory of Bioresources, Biotechnology, Ethnopharmacology and Health, Univ. Mohammed Premier of Oujda. The culture media used for their culture were Mueller–Hinton medium (BIOKAR, Allonne, France) for bacteria and Potato Dextrose Agar (PDA) (BIOKAR, Allonne, France) for fungi.

4.2. Measurement of Antibacterial and Antifungal Activities

The solid-medium diffusion method (Mueller–Hinton medium) was used to determine antibacterial activity against bacteria (*Listeria innocua*, *E. coli*, *Pseudomonas aeruginosa*, and *Staphylococcus aureus*), and *Potato Dextrose Agar medium* (BIOKAR, France) for antifungal activity against *Asperillus niger*, *Geotrichum candidum*, and *Penicillium crustosum*. The strains were diluted and adjusted to 0.5 McFarland, which corresponds to 10^6 CFU/mL for bacteria and 10^6 spores/mL for molds. Cultures were diluted with Mueller–Hinton broth for bacteria, and with sterile physiological water for molds. An amount of 0.1 mL of each diluted strain was inoculated by surface spreading of the solid culture medium corresponding to each type of microorganism (bacteria or mold). An amount of 100 μ L of each sample at a concentration of 6 mg/mL (DMSO) was filled into the wells made on the solid medium. The dishes were then incubated for 2 h at 4 °C and then at 37 °C for 24 h for bacteria and at 25 °C for fungi. The diameters of the inhibition zones obtained around the wells were measured. Cycloheximide and Gentamicin were used as positive controls against fungi and bacteria, respectively.

4.3. Antifungal Activity on Mycelial Growth of *Fusarium oxysporum*

Fusarium oxysporum isolates were obtained from xylem tissues showing typical “Bay-oud” symptoms on Boufegousgharas date palm in Figuig, Morocco. Small vascular tissue fragments were removed and placed in sterile PDA medium, then incubated at 28 °C. The identification of *Fusarium oxysporum* isolates was carried out by observing their morphological features [55,56]. Following incubation on PDA medium at 28 °C, a single monoconidial *Fusarium oxysporum* was isolated.

A total of 4 mg of each molecule was dissolved in DMSO (1 mL). From this solution, 50 μ L and 150 μ L were placed in sterile tubes. Then, the sterile liquid PDA was added until reaching a total volume of 10 mL. The entire set was placed on Petri dishes with 8.5 cm diameter, and the medium was allowed to stand until solidification [51]. In the middle of each Petri dish was a pellet of FOA that had already grown on the solid PDA. The dishes were incubated for four days at 28 °C. By comparing the diameter of the FOA to a control that contained only DMSO at some dose (control), the results are reported as a percentage of inhibition as follows [52]:

$$\% \text{ of inhibition} = \frac{D_0 - D_x}{D_0} \times 100$$

D_0 = diameter (cm) of the FOA in the control.

D_x = diameter (cm) of the FOA in the test.

4.4. Genotoxicity Effect

To obtain blood samples, rats were anesthetized using pentobarbital, and samples were collected retro-orbitally using heparin-containing tubes. The collected blood (2 mL) from a male Wistar rat was mixed with an equal volume (2 mL) of Ca^{II} - and Mg^{II} -free phosphate-buffered saline (PBS) solutions (137 mM NaCl; 2.7 mM KCl; 10 mM Na_2HPO_4 ; 1.76 mM KH_2PO_4 ; pH 7.4). The diluted blood was then exposed to the samples. The samples were dissolved in PBS to achieve the desired concentrations (5 and 10 $\mu\text{g}/\text{mL}$). Subsequently, the diluted blood samples were incubated with the respective samples for two hours at 37 °C. The negative control was exposed to PBS, while hydrogen peroxide (250 $\mu\text{mol}/\text{L}$) was used as the positive control.

The comet assay, also known as the single-cell gel electrophoresis assay, is a commonly used technique to evaluate genotoxicity. It measures DNA damage in individual cells by visualizing the migration of fragmented DNA under an electric field. Several parameters are assessed in the comet assay, including tail moment, tail intensity, and tail length, which provide information about the extent and severity of DNA damage. Higher values of tail moment, tail intensity, and tail length indicate more significant genotoxic effects [57–60].

A modified version of the alkaline comet test protocol described in [61] was implemented with minor adjustments. Following treatment, the suspension was centrifuged at 4500 rpm for 10 min. The pellet containing leukocytes was then dissolved in PBS (1 mL) after removing the supernatant. The washing process was repeated three times. Subsequently, the pellet was dissolved in a solution of low-melting-point (LMP) agarose (0.5% *w/v* in PBS). The resulting mixture was applied to a slide previously coated with normal-melting-point (NMP) agarose (1.5% *w/v*). The slides were immersed in a lysis solution (2.5 M NaCl, 100 mM Na₂EDTA, 20 mM Tris, 300 mM NaOH, 1% N-lauroylsarcosine sodium, 10% DMSO, and 1% Triton X-100) for 5 min, followed by 1 h of incubation in the dark at 4 °C. After the lysis period, the slides were thoroughly washed with double-distilled water. The slides were then placed in horizontal gel electrophoresis apparatus with an electrophoresis solution consisting of 300 mM NaOH and 1 mM Na₂EDTA at pH 13. DNA unravelling was performed for 20 min at a constant current of 300 mA and a set voltage of 25 V. The temperature of the electrophoresis solution was maintained at 4 °C throughout the run. Following electrophoresis, the slides were immersed in a neutralization buffer (400 mM Trizma solution adjusted to pH 7.5 using HCl) for 5 min. This process was repeated three times. Finally, the comets were visualized using the ethidium bromide staining method [62].

The ethidium-bromide-stained slides were observed and captured using ZOE Cell Imager fluorescence microscopy, specifically utilizing the red channel with an excitation wavelength of 556/20 nm and an emission wavelength of 615/61 nm. To quantitatively estimate DNA damage, an image analyzer coupled with processing software was employed. In this study, Comet Assay IV image analysis software was utilized, enabling the quantification of various parameters associated with DNA lesions [63]. Two replicates were conducted for each sample, and a total of fifty cells were randomly selected for analysis in each replicate.

4.5. Statistical Analysis

Statistical analysis was performed using GraphPad Prism V9 software. A one-way ANOVA was utilized to assess the statistical significance of the data. Differences between treatment groups were examined using Tukey's honest significance test, with significance thresholds set at $p < 0.05$, $p < 0.01$, $p < 0.001$, and $p < 0.0001$.

5. Conclusions

In this work, we have prepared two new molecules, 1,5-dimethyl-*N*-phenyl-1H-pyrazole-3-carboxamide (**L**₁) and 1,5-dimethyl-*N*-propyl-1H-pyrazole-3-carboxamide (**L**₂), based on pyrazoles and amides. Their reactivity with nickel and cadmium salts led to two complexes **C**₁ and **C**₂. We further support our study with biological investigations that showcased our coordination complexes as potential antibacterial and antifungal agents. We demonstrated that **C**₂ has a remarkable antifungal activity compared to cycloheximide. This Cd coordination complex also exhibits a remarkable anti-*Fusarium* activity (96% inhibition) against *Fusarium Oxysporum* f. sp. *Albedinis*. We also investigated the genotoxicity of our ligands and coordination complexes using the comet assay, where we demonstrated that the addition of metal ions increased the genotoxicity, as expected, compared to our ligands. We believe that the development of less genotoxic coordination compounds with a high biological activity is an ideal future research direction.

Supplementary Materials: The following supporting information can be downloaded at: <https://www.mdpi.com/article/10.3390/molecules29051186/s1>, Figures S1–S4: NMR spectroscopy of **L**₁, **L**₂, **C**₁, **C**₂. Figures S5–S8: mass spectroscopy of **L**₁, **L**₂, **C**₁, **C**₂.

Author Contributions: A.E.M. performed synthesis, characterization and wrote the paper with Y.G. and K.R.; S.R. and Y.G. both designed and managed the project; M.E.M. and Y.D. contributed to some organic syntheses; K.R. undertook X-ray studies; S.O., A.A., N.E.B., E.S. and R.B. performed biological experiments; All authors have read and agreed to the published version of the manuscript.

Funding: This research was supported by the Fonds de la Recherche Scientifique—FNRS (PDR T.0095.21, CDR J.0064.23, J.0168.22, EQP U.N027.24), CNRST (PPR2-MESRSFC-CNRSTP10) and the COST action CA21149.

Institutional Review Board Statement: Not applicable.

Informed Consent Statement: Not applicable.

Data Availability Statement: Data are contained within the article and Supplementary Materials.

Acknowledgments: We thank WBI Morocco for granting a research stay for A.E.M. in Belgium. We thank the chemistry department at the University of Aveiro for providing mass spectral data and A. Talhaoui and staff members for open access to the analytical platform of the Faculty of Sciences of Oujda.

Conflicts of Interest: The authors declare no conflict of interest.

References

1. Cattoir, V.; Felden, B. Future Antibacterial Strategies: From Basic Concepts to Clinical Challenges. *J. Infect. Dis.* **2019**, *220*, 350–360. [[CrossRef](#)] [[PubMed](#)]
2. World Health Organization. *2021 Antibacterial Agents in Clinical and Preclinical Development: An Overview and Analysis*; World Health Organization: Geneva, Switzerland, 2021.
3. Frei, A.; Zuegg, J.; Elliott, A.G.; Baker, M.; Braese, S.; Brown, C.; Chen, F.; Dowson, C.G.; Dujardin, G.; Jung, N.; et al. Metal Complexes as a Promising Source for New Antibiotics. *Chem. Sci.* **2020**, *11*, 2627–2639. [[CrossRef](#)] [[PubMed](#)]
4. Swiatoslaw, T. Coordination Chemistry of Pyrazole-Derived Ligands. *Chem. Rev.* **1972**, *72*, 497–509. [[CrossRef](#)]
5. Ebenezer, O.; Shapi, M.; Tuszynski, J.A. A Review of the Recent Development in the Synthesis and Biological Evaluations of Pyrazole Derivatives. *Biomedicines* **2022**, *10*, 1124. [[CrossRef](#)] [[PubMed](#)]
6. Draoui, Y.; Radi, S.; Tanan, A.; Oulmidi, A.; Miras, H.N.; Benabbes, R.; Ouahhoudo, S.; Mamri, S.; Rotaru, A.; Garcia, Y. Novel Family of Bis-Pyrazole Coordination Complexes as Potent Antibacterial and Antifungal Agents. *RSC Adv.* **2022**, *12*, 17755–17764. [[CrossRef](#)]
7. Oulmidi, A.; Rotaru, A.; Radi, S.; Garcia, Y. Pyrazole's Substituents Effect on the Spin State of [Fe(Bpp)₂]²⁺ complexes. *Hyperfine Interact.* **2021**, *242*, 8. [[CrossRef](#)]
8. Oulmidi, A.; Radi, S.; Miras, H.N.; Adarsh, N.N.; Garcia, Y. New Bis-Pyrazole-Bis-Acetate Based Coordination Complexes: Influence of Counter-Anions and Metal Ions on the Supramolecular Structures. *Sustainability* **2020**, *13*, 288. [[CrossRef](#)]
9. Radi, S.; El-Massaoudi, M.; Benaissa, H.; Adarsh, N.N.; Ferbinteanu, M.; Devlin, E.; Sanakis, Y.; Garcia, Y. Crystal Engineering of a Series of Complexes and Coordination Polymers Based on Pyrazole-Carboxylic Acid Ligands. *New J. Chem.* **2017**, *41*, 8232–8241. [[CrossRef](#)]
10. Chkirate, K.; Karrouchi, K.; Dege, N.; Kheira Sebbar, N.; Ejjoummany, A.; Radi, S.; Adarsh, N.N.; Talbaoui, A.; Ferbinteanu, M.; Essassi, E.M.; et al. Co(II) and Zn(II) Pyrazolyl-Benzimidazole Complexes with Remarkable Antibacterial Activity. *New J. Chem.* **2020**, *44*, 2210–2221. [[CrossRef](#)]
11. Chkirate, K.; Karrouchi, K.; Chakchak, H.; Mague, J.T.; Radi, S.; Adarsh, N.N.; Li, W.; Talbaoui, A.; Essassi, E.M.; Garcia, Y. Coordination Complexes Constructed from Pyrazole–Acetamide and Pyrazole–Quinoxaline: Effect of Hydrogen Bonding on the Self-Assembly Process and Antibacterial Activity. *RSC Adv.* **2022**, *12*, 5324–5339. [[CrossRef](#)]
12. Chkirate, K.; Fettach, S.; Karrouchi, K.; Sebbar, N.K.; Essassi, E.M.; Mague, J.T.; Radi, S.; El Abbes Faouzi, M.; Adarsh, N.N.; Garcia, Y. Novel Co(II) and Cu(II) Coordination Complexes Constructed from Pyrazole–Acetamide: Effect of Hydrogen Bonding on the Self Assembly Process and Antioxidant Activity. *J. Inorg. Biochem.* **2019**, *191*, 21–28. [[CrossRef](#)]
13. Malek, F.; Ramdani, A.; Zidane, I.; Yahyi, A.; Radi, S. Tetrapyrazolic Tripods. Synthesis and Preliminary Use in Metal Ion Extraction. *Tetrahedron* **2005**, *61*, 2995–2998. [[CrossRef](#)]
14. Malek, F.; Ramdani, A.; Radi, S. Pyrazolic Tripods Synthesis and Cation Binding Properties. *J. Chem. Res.* **2004**, *2004*, 640–641. [[CrossRef](#)]
15. Radi, S.; Ramdani, A.; Lekchiri, Y.; Morcellet, M.; Crini, G.; Janus, L.; Martel, B. Extraction of Metal Ions from Water with Tetrapyrazolic Macrocycles Bound to Merrifield Resin and Silica Gel. *J. Appl. Polym. Sci.* **2000**, *78*, 2495–2499. [[CrossRef](#)]
16. Mouadili, A.; Attayibat, A.; Kadiri, S.E.; Radi, S.; Touzani, R. Catecholase Activity Investigations Using in Situ Copper Complexes with Pyrazole and Pyridine Based Ligands. *Appl. Catal. A Gen.* **2013**, *454*, 93–99. [[CrossRef](#)]
17. Radi, S.; Tighadouini, S.; Toubi, Y.; Bacquet, M. Polysiloxane Surface Modified with Bipyrazolic Tripodal Receptor for Quantitative Lead Adsorption. *J. Hazard. Mater.* **2011**, *185*, 494–501. [[CrossRef](#)] [[PubMed](#)]
18. Radi, S.; Tighadouini, S.; Bacquet, M.; Degoutin, S.; Janus, L.; Mabkhot, Y.N. Fabrication and Covalent Modification of Highly Chelated Hybrid Material Based on Silica-Bipyridine Framework for Efficient Adsorption of Heavy Metals: Isotherms, Kinetics and Thermodynamics Studies. *RSC Adv.* **2016**, *6*, 82505–82514. [[CrossRef](#)]

19. Radi, S.; El Abiad, C.; Carvalho, A.P.; Santos, S.M.; Faustino, M.A.F.; Neves, M.G.P.M.S.; Moura, N.M.M. An Efficient Hybrid Adsorbent Based on Silica-Supported Amino Penta-Carboxylic Acid for Water Purification. *J. Mater. Chem. A* **2018**, *6*, 13096–13109. [[CrossRef](#)]
20. Radi, S.; Toubi, Y.; El-Massaoudi, M.; Bacquet, M.; Degoutin, S.; Mabkhot, Y.N. Efficient Extraction of Heavy Metals from Aqueous Solution by Novel Hybrid Material Based on Silica Particles Bearing New Schiff Base Receptor. *J. Mol. Liq.* **2016**, *223*, 112–118. [[CrossRef](#)]
21. Radi, S.; Attayibat, A.; Ramdani, A.; Bacquet, M. Synthesis and Characterization of Novel Silica Gel Supported N-Pyrazole Ligand for Selective Elimination of Hg(II). *Eur. Polym. J.* **2008**, *44*, 3163–3168. [[CrossRef](#)]
22. Cherrak, K.; Belghiti, M.E.; Berrissoul, A.; El Massaoudi, M.; El Faydy, M.; Taleb, M.; Radi, S.; Zarrouk, A.; Dafali, A. Pyrazole Carbohydrazide as Corrosion Inhibitor for Mild Steel in HCl Medium: Experimental and Theoretical Investigations. *Surf. Interfaces* **2020**, *20*, 100578. [[CrossRef](#)]
23. Belghiti, M.; Tighadouini, S.; Karzazi, Y.; Dafali, A.; Hammouti, B.; Radi, S.; Solmaz, R. New Hydrazine Derivatives as Corrosion Inhibitors for Mild Steel Protection in Phosphoric Acid Medium. Part A: Experimental Study. *J. Mater. Environ. Sci.* **2016**, *7*, 337–346.
24. Oulmidi, A.; Radi, S.; Idir, A.; Zyad, A.; Kabach, I.; Nhiri, M.; Robeyns, K.; Rotaru, A.; Garcia, Y. Synthesis and Cytotoxicity against Tumor Cells of Pincer N-Heterocyclic Ligands and Their Transition Metal Complexes. *RSC Adv.* **2021**, *11*, 34742–34753. [[CrossRef](#)]
25. Ronco, C.; Martin, A.R.; Demange, L.; Benhida, R. ATM, ATR, CHK1, CHK2 and WEE1 Inhibitors in Cancer and Cancer Stem Cells. *Med. Chem. Commun.* **2017**, *8*, 295–319. [[CrossRef](#)]
26. Radi, S.; Salhi, S.; Radi, A. Synthesis and Preliminary Biological Activity of Some New Pyrazole Derivatives as Acyclonucleoside Analogues. *Lett. Drug Des. Discov.* **2010**, *7*, 27–30. [[CrossRef](#)]
27. Mabkhot, Y.; Al-Majid, A.; Barakat, A.; Al-Showiman, S.; Al-Har, M.; Radi, S.; Naseer, M.; Hadda, T. Synthesis and Biological Evaluation of 2-Aminobenzamide Derivatives as Antimicrobial Agents: Opening/Closing Pharmacophore Site. *Int. J. Mol. Sci.* **2014**, *15*, 5115–5127. [[CrossRef](#)]
28. Karrouchi, K.; Fettach, S.; Anouar, E.H.; Tüzün, B.; Radi, S.; Alharthi, A.I.; Ghabbour, H.A.; Mabkhot, Y.N.; Faouzi, M.E.A.; Ansar, M.; et al. Synthesis, Crystal Structure, DFT, α -Glucosidase and α -Amylase Inhibition and Molecular Docking Studies of (E)-N'-(4-Chlorobenzylidene)-5-Phenyl-1H-Pyrazole-3-Carbohydrazide. *J. Mol. Struct.* **2021**, *1245*, 131067. [[CrossRef](#)]
29. Cetin, A.; Kurt, H. Synthesis, Antibacterial Activity and Molecular Docking Studies of New Pyrazole Derivatives. *Lett. Drug Des. Discov.* **2020**, *17*, 745–756. [[CrossRef](#)]
30. Karrouchi, K.; Radi, S.; Ramli, Y.; Taoufik, J.; Mabkhot, Y.; Al-aizari, F.; Ansar, M. Synthesis and Pharmacological Activities of Pyrazole Derivatives: A Review. *Molecules* **2018**, *23*, 134. [[CrossRef](#)] [[PubMed](#)]
31. Rajput, A.; Mukherjee, R. Coordination Chemistry with Pyridine/Pyrazine Amide Ligands. Some Noteworthy Results. *Coord. Chem. Rev.* **2013**, *257*, 350–368. [[CrossRef](#)]
32. Draoui, Y.; Radi, S.; El Massaoudi, M.; Bahjou, Y.; Ouahhoud, S.; Mamri, S.; Ferbinteanu, M.; Benabbes, R.; Wolff, M.; Robeyns, K.; et al. Coordination Complexes Built from a Ditopic Triazole-Pyrazole Ligand with Antibacterial and Antifungal Performances. *Molecules* **2023**, *28*, 6801. [[CrossRef](#)]
33. Preti, C.; Tosi, G.; Filippo, D.D.; Verani, G. Cobalt(II) and Nickel(II) Complexes with Nitrogen, Sulfur, and Selenium Containing Heterocyclic Ligands. *Can. J. Chem.* **1974**, *52*, 2021–2028. [[CrossRef](#)]
34. Popović, Z.V.; Stanišić, G.; Stojanović, D.; Kostić, R. Infrared and Raman Spectra of CdO. *Phys. Status Solidi B* **1991**, *165*, K109–K112. [[CrossRef](#)]
35. Kamath, P.V.; Ganguly, S. Infrared Spectroscopic Studies of the Oxide-Hydroxides of Ni, Co and Mn. *Mater. Lett.* **1991**, *10*, 537–539. [[CrossRef](#)]
36. Ali, I.; Wani, W.A.; Khan, A.; Haque, A.; Ahmad, A.; Saleem, K.; Manzoor, N. Synthesis and Synergistic Antifungal Activities of a Pyrazoline Based Ligand and Its Copper(II) and Nickel(II) Complexes with Conventional Antifungals. *Microb. Pathog.* **2012**, *53*, 66–73. [[CrossRef](#)] [[PubMed](#)]
37. You, Z.; Zhu, H. Syntheses, Crystal Structures, and Antibacterial Activities of Four Schiff Base Copper(II), Zinc(II), and Cadmium(II) Complexes Derived from 2-[(2-Dimethylaminoethylimino)Methyl]Phenol. *Z. Anorg. Allg. Chem.* **2006**, *632*, 140–146. [[CrossRef](#)]
38. Bahjou, Y.; Radi, S.; El Massaoudi, M.; Draoui, Y.; Adarsh, N.N.; Miras, H.N.; Ferbinteanu, M.; Robeyns, K.; Ouahhoud, S.; Benabbes, R.; et al. High Inhibition for a Co^{II} Tetrazole Bi-pyrazole Dinuclear Complex against *Fusarium Oxysporum* f. Sp. *Albedinis*. *Eur. J. Inorg. Chem.* **2023**, e202300634. [[CrossRef](#)]
39. Biswas, F.B.; Roy, T.G.; Rahman, M.A.; Emran, T.B. An in Vitro Antibacterial and Antifungal Effects of Cadmium(II) Complexes of Hexamethyltetraazacyclotetradecadiene and Isomers of Its Saturated Analogue. *Asian Pac. J. Trop. Med.* **2014**, *7*, S534–S539. [[CrossRef](#)] [[PubMed](#)]
40. Dal Pizzol, M.; Freitas, E.C.; Locatelli, C.; Guareze, F.; Reginatto, P.; Machado, G.; Fuentefria, A.; Marinho, D. Antifungal Efficacy and Safety of Cycloheximide as a Supplement in Optisol-GS. *Lett. Drug Des. Discov.* **2021**, *15*, 2091–2098. [[CrossRef](#)] [[PubMed](#)]
41. Mohamed, G.; Hassan, F.; Hossainy, A.; Khidr, M. Coordination Behaviour and Biological Activity Studies of Transition Metal Complexes with Indapamide and Mixed Ligands of Indapamide and Glycine. *J. Pharm.* **2012**, *20125*, 3753–3763.

42. Montazerzohori, M.; Zahedi, S.; Nasr-Esfahani, M.; Naghiha, A. Some New Cadmium Complexes: Antibacterial/Antifungal Activity and Thermal Behavior. *J. Ind. Eng. Chem.* **2014**, *20*, 2463–2470. [[CrossRef](#)]
43. Chandra, S.; Vandana; Kumar, S. Synthesis, Spectroscopic, Anticancer, Antibacterial and Antifungal Studies of Ni(II) and Cu(II) Complexes with Hydrazine Carboxamide, 2-[3-Methyl-2-Thienyl Methylene]. *Spectrochim. Acta Part A Mol. Biomol. Spectrosc.* **2015**, *135*, 356–363. [[CrossRef](#)]
44. Bahjou, Y.; Draoui, Y.; Radi, S.; Robeyns, K.; Li, W.; Miras, H.N.; Ferbinteanu, M.; Bentouhami, N.E.; Asehrou, A.; Rotaru, A.; et al. A Cu(II) Coordination Polymer as a Robust Inhibitor of *Fusarium Oxysporum* f. Sp. *Albedinis*; LCAE, Department of Chemistry, Faculty of Sciences, University Mohammed I: Oujda, Morocco, 2024; submitted.
45. Islam, M.R.; Islam, S.M.R.; Noman, A.S.M.; Khanam, J.A.; Ali, S.M.M.; Alam, S.; Lee, M.-W. Biological Screening of a Novel Nickel (II) Tyrosine Complex. *Mycobiology* **2007**, *35*, 25–29. [[CrossRef](#)]
46. Tighadouini, S.; Radi, S.; Abridgach, F.; Benabbes, R.; Eddike, D.; Tillard, M. Novel β -Keto–Enol Pyrazolic Compounds as Potent Antifungal Agents. Design, Synthesis, Crystal Structure, DFT, Homology Modeling, and Docking Studies. *J. Chem. Inf. Model.* **2019**, *59*, 1398–1409. [[CrossRef](#)] [[PubMed](#)]
47. Kaddouri, Y.; Abridgach, F.; Ouahhoud, S.; Benabbes, R.; El Kodadi, M.; Alsalmé, A.; Al-Zaqri, N.; Warad, I.; Touzani, R. Mono-Alkylated Ligands Based on Pyrazole and Triazole Derivatives Tested against *Fusarium Oxysporum* f. Sp. *Albedinis*: Synthesis, Characterization, DFT, and Phytase Binding Site Identification Using Blind Docking/Virtual Screening for Potent Fophy Inhibitors. *Front. Chem.* **2020**, *8*, 559262. [[CrossRef](#)] [[PubMed](#)]
48. Benhusein, G.; Mutch, E.; Aburawi, S.; Williams, F. Genotoxic Effect Induced by Hydrogen Peroxide in Human Hepatoma Cells Using Comet Assay. *Libyan J. Med.* **2010**, *5*, 4637. [[CrossRef](#)]
49. El-Habit, O.H.; Abdel Moneim, A.E. Testing the Genotoxicity, Cytotoxicity, and Oxidative Stress of Cadmium and Nickel and Their Additive Effect in Male Mice. *Biol. Trace Elem. Res.* **2014**, *159*, 364–372. [[CrossRef](#)]
50. Permenter, M.G.; Lewis, J.A.; Jackson, D.A. Exposure to Nickel, Chromium, or Cadmium Causes Distinct Changes in the Gene Expression Patterns of a Rat Liver Derived Cell Line. *PLoS ONE* **2011**, *6*, e27730. [[CrossRef](#)]
51. Cameron, K.S.; Buchner, V.; Tchounwou, P.B. Exploring the Molecular Mechanisms of Nickel-Induced Genotoxicity and Carcinogenicity: A Literature Review. *Rev. Environ. Health* **2011**, *26*, 81–92. [[CrossRef](#)]
52. Agilent Technologies. *CrysAlisPro*, V 1.171. 37.35; Agilent Technologies: Santa Clara, CA, USA, 2014.
53. Sheldrick, G.M. SHELXT—Integrated Space-Group and Crystal-Structure Determination. *Acta Crystallogr. A Found. Adv.* **2015**, *71*, 3–8. [[CrossRef](#)]
54. Sheldrick, G.M. Crystal Structure Refinement with SHELXL. *Acta Crystallogr. C Struct. Chem.* **2015**, *71*, 3–8. [[CrossRef](#)]
55. Nelson, P.E.; Toussoun, T.A.; Cook, R.J. (Eds.) *Fusarium: Diseases, Biology, and Taxonomy*; Pennsylvania State University Press: University Park, PA, USA, 1981; ISBN 978-0-271-00293-4.
56. Booth, C. *The Genus Fusarium*; Commonwealth Agricultural Bureaux [for the] Commonwealth Mycological Institute: Farnham Royal, UK, 1971; ISBN 978-0-85198-046-1.
57. Rossi, R.; Ciofalo, M. An Updated Review on the Synthesis and Antibacterial Activity of Molecular Hybrids and Conjugates Bearing Imidazole Moiety. *Molecules* **2020**, *25*, 5133. [[CrossRef](#)] [[PubMed](#)]
58. Tice, R.R.; Agurell, E.; Anderson, D.; Burlinson, B.; Hartmann, A.; Kobayashi, H.; Miyamae, Y.; Rojas, E.; Ryu, J.-C.; Sasaki, Y.F. Single Cell Gel/Comet Assay: Guidelines for in Vitro and in Vivo Genetic Toxicology Testing. *Environ. Mol. Mutagen.* **2000**, *35*, 206–221. [[CrossRef](#)]
59. Collins, A.R. The Comet Assay for DNA Damage and Repair: Principles, Applications, and Limitations. *MB* **2004**, *26*, 249–261. [[CrossRef](#)] [[PubMed](#)]
60. Olive, P.L.; Banáth, J.P.; Durand, R.E. Heterogeneity in Radiation-Induced DNA Damage and Repair in Tumor and Normal Cells Measured Using the “Comet” Assay. *Radiat. Res.* **2012**, *178*, AV35–AV42. [[CrossRef](#)] [[PubMed](#)]
61. Ouahhoud, S.; Khoulati, A.; Kadda, S.; Bencheikh, N.; Mamri, S.; Ziani, A.; Baddaoui, S.; Eddabbeh, F.-E.; Lahmass, I.; Benabbes, R.; et al. Antioxidant Activity, Metal Chelating Ability and DNA Protective Effect of the Hydroethanolic Extracts of *Crocus Sativus* Stigmas, Tepals and Leaves. *Antioxidants* **2022**, *11*, 932. [[CrossRef](#)]
62. Singh, N.P.; McCoy, M.T.; Tice, R.R.; Schneider, E.L. A Simple Technique for Quantitation of Low Levels of DNA Damage in Individual Cells. *Exp. Cell Res.* **1988**, *175*, 184–191. [[CrossRef](#)]
63. Strubbia, S.; Lyons, B.P.; Lee, R.J. Spatial and Temporal Variation of Three Biomarkers in *Mytilus Edulis*. *Mar. Pollut. Bull.* **2019**, *138*, 322–327. [[CrossRef](#)]

Disclaimer/Publisher’s Note: The statements, opinions and data contained in all publications are solely those of the individual author(s) and contributor(s) and not of MDPI and/or the editor(s). MDPI and/or the editor(s) disclaim responsibility for any injury to people or property resulting from any ideas, methods, instructions or products referred to in the content.